Exhibit A

(Part 4)

ment are well defined (Fig. 1(a)) and the target gas is essentially limited to the QUAD 2 region so that the system is well suited for these measurements. It has been operated without apertures between the three quadrupoles but some experiments are also described below where inter-quadrupole plates were inserted with apertures of diameter $1.4r_0$. In all cases, the ions remained continuously in the r.f. field in contrast to those instruments where ions leave and re-enter the field between quadrupoles and suffer the effects of the fringing fields [12]. Measurements were made on both positive and negative ions. Detection of ions was by counting.

Fig. 3. Phase space acceptance ellipses for various phases of a 'long' quadrupole field for (a) $a = 0, q = 0.1$, (b) $a = 0, q = 0.6$ and (c) $a = 0, q = 0.85$.

CONTAINMENT OF PARENT IONS

Dependence on q_p

The ion acceptance of QUAD 2, ϵ, was calculated as a function of q when $a = 0$. The results are shown in Fig. 4. Since there are acceptances in two transverse directions to consider, ϵ^2 is also shown. The figure illustrates that mathematical stability of the ion trajectories is not the sole criterion in ion containment but that the choice of the q value (r.f. amplitude) is important.

The ion acceptance was measured as a function of the applied r.f. voltage on QUAD 2 for a triple quadrupole without interquadrupole apertures for the protonated parent ions of a phosphorus ester, dimethylmorpholinophosphoramidate (DMMPA) of mass 186 and its various daughter ions of masses 86, 42 and 15 produced by dissociation in collision with nitrogen [7]. The results are summarized in Fig. 5. The storage of the daughters was found to depend primarily on the efficiency of storage of the parent (i.e. on q_p) until the q_d reached about 0.7 when daughter containment decreased. The problems of daughter containment are discussed below. The results of Fig. 5 strongly suggest that when $q_d < 0.7$, the trapping of daughter ions is very efficient and the daughters can also be observed as a measure of efficiency of parent storage. Daughters differ from parents in that they are formed throughout the length of QUAD 2, although their formation is concentrated towards the centre.

Parent ions enter QUAD 2 from QUAD 1 and one concern in designing

Fig. 4. Acceptance of the central r_1 only quadrupole as a function of q (i.e. of r_1 voltage). r_2 takes into account both transverse directions.

Fig. 5. Stability of various daughters of $m/z = 199$ as a function of the q of the parent ion.

Fig. 6. Transmission of $H(H_2O)_3^+$ parent ions as a function of the q value when intersquadrupole plates with apertures of $1.4r_0$ are used.

Fig. 7. Plots of the q values for maxima and minima in transmission for parent ions of three different axial velocities: (a) $M = 37$, $E = 35$; (b) $M = 55$, $E = 35$; and (c) $M = 55$, $E = 20$

Fig. 8. Transmission of $m/z = 37$ and 19 daughter ions as a function of the q of the parent $H(H_2O)_3^+$ ion. The solid line is the calculation of ζ^2 normalized at $q_p = 0.98$.

triple quadrupoles is the existence of ion focusing effects in QUAD 2 and their influence on the observed spectra. Quadrupole fields have very strong focusing properties [12,16]. If the source of ions into QUAD 2 is restricted in size, imaging of the source on the entrance to QUAD 3 whenever $\beta_{x,y} = p/n$ (where $p = 1, 2, 3, \ldots$ and n is the number of field cycles) can be expected because of the nature of the fundamental ion oscillation. If the parent ions have a sufficiently well-defined axial energy, the focusing effects will be observed in the parent ion transmission when restrictive apertures are present between the quadrupoles. Figure 6 shows transmission measurements of the $H(H_2O)_3^+$ ion of 20 ± 2 eV energy in a triple quadrupole with apertures of diameter $1.4r_0$ between each set of quadrupoles. When q is small, $\beta \approx q/\sqrt{2}$, and the maxima and minima are spaced evenly as would be predicted from the focusing theory. (Similar structures can also be observed in a normal single quadrupole under appropriate conditions [17]). The focusing effects will only be observed so dramatically if the axial ion energy spread is small although with a large energy spread the losses in ion transmission would, of course, still be present at a wider range of q values. It was verified by experiment, as illustrated in Fig. 7, that the focusing maxima and minima depend upon the axial velocity and therefore upon parent ion mass and axial energy. There have been some calculations published recently [18] for quadrupoles with smaller apertures.

Even when the parent ion beam is defocused at the exit from QUAD 2 and its transmission is decreased, daughter ions can still be efficiently formed

and transmitted into QUAD 3. Figure 8 shows the transmission of $M = 37$ and $M = 19$ daughter ions formed from $M = 55$ as a function of q_{z_1}. The solid line represents the calculated variation of the acceptance of QUAD 2, ϵ'. The experimental data have been normalized at $q_{z_1} = 0.08$. The daughter ions show only very minor reflections of the focusing effects observed in the parent beam. The only problem is in the transmission of parents at the exit from QUAD 2 to QUAD 3. The experiment is in excellent agreement with the calculation. The parent peak shows the same overall shape with the focusing effects superimposed. Up to q of about 0.1, the transmission is limited by the acceptance of QUAD 2 but above that value it is almost constant and the limitation is the emissivity of the source plus QUAD 1.

If the triple quadrupole is operated in the constant q daughter scanning mode and the ratio of $(r.f.)_2/(r.f.)_1$ is chosen to be relatively high (e.g. 0.5–0.8), then the focusing effects will have little influence on either parent or daughter observation with this aperture size. Measurements such as those of Fig. 8 serve as a check on the constancy of parent ion transmissivity during daughter ion measurement. In the example given, transmissivity is constant for q_p greater than about 0.1. That is, no transmission corrections are necessary as long as $M_{daughter} > (M_{parent}/7)$ $((r.f.)_2/(r.f.)_1)$. Below this mass, Fig. 8 can be used as a calibration curve, when quantitative measurements are required.

In the constant q parent mode of scanning, q_p has to be set at a low value in order to have a sufficient range of daughter masses within the stability region. A q_p of 0.1–0.2 might be typical. However, observations of the different parents may then be distorted by focusing effects. A similar problem arises if the (r.f.)$_2$ is simply held constant. The focusing effects will be much more severe than those of Fig. 6. If the apertures between the quadrupoles are small or if there are a series of restricting apertures as is the case in some instruments.

Effect of velocity changes on ion containment

The observation of loss of parents and formation of daughters in collisional fragmentation might be limited by scattering in non-fragmenting collisions. It is important to have some estimate of this effect (for example, to estimate the lowest value of dissociation cross-section that might be observable). It is also important to verify that ion loss by simple scattering is small, if quantitative measurements of ion kinetics are to be accepted.

Sudden changes in transverse velocity due to collision are best examined in terms of the acceptance ellipses at different q values (Fig. 3). Consider for example, a sudden decrease in transverse velocity assuming initially that the acceptance ellipses are uniformly occupied. A decrease in transverse velocity can have a stabilizing or destabilizing effect on the ion trajectory depending upon the phase of the r.f. field at the moment of collision, the value of u, u and the value of q_p. At the so-called 'zero' phase of the field, the acceptance ellipse is always oriented along the u axis and any decrease in transverse velocity is stabilizing for any allowed u, u value (since the uu value is moved to a point on a smaller ellipse). The same is true at the $\xi_0 = \pi/2$ phase when the ellipse has a similar orientation. At intermediate phases, however, some of the allowed uu values of the ions will be transformed to points outside the ellipses and these ions will eventually be lost from QUAD 2. The techniques of calculation were given in an earlier publication [19] concerning sudden reductions of velocity to zero (charge exchange) in the three-dimensional ion trap. Here the losses over twenty different phases of the r.f. field have been averaged in order to examine ion loss as a function of q. It is evident from an examination of the ellipses of Fig. 3 that a sudden decrease in transverse velocity is much more serious at $q = 0.85$ than at $q = 0.1$. Figure 9 summarizes the results on ion loss for a reduction in velocity by (a) 25% and (b) 50%. The losses go to 100% at the limit of ion stability at $q = 0.91$. Only one section that a typical instrument might have in acceptance occupied only up to the value at $q_p = \sim 0.1$, a calculation for this value of the acceptance was also carried out, and the reduced ion loss is indicated on Fig. 9 as curve (c). This is the more realistic situation with appreciable loss only below $q = 0.2$ and above $q = 0.75$.

The ions that remain confined after a collision are generally stabilized and subsequent collisions are less effective in causing destabilization. For example, at $q = 0.6$, it was shown [19] that a first collision reducing the transverse velocity to zero would lead to an ion loss of 23% but a second such collision would lead to only an additional 7% loss.

The noticeable feature of Fig. 9 is the very small ion loss that is experienced when q_p is below about 0.8, even for these rather large changes in velocity. Standard conditions for the accumulation of library spectra for CID in triple quadrupoles have been suggested as a 63% reduction in the parent intensity [7,8].

Since in a scattering event, some of the axial energy might become transformed into transverse energy, increases in transverse velocity must also be considered. Figure 9 also includes results for this situation, labelled curves (d) and (e). An increase in velocity is destabilizing for all initial phases. The curves are for an increase of 25%. Curve (d) was calculated under the artificial assumption that the acceptance is fully occupied at all q values. Curve (e) corresponds more closely to the experimental measurements discussed above where the occupied acceptance is equal to that for $q = 0.1$. The coning of each instrument design can be.

Some experimental measurements were made using O^- ($M = 16$) colliding with argon at a laboratory energy of about 55 eV. The results are shown in Fig. 10 (curve (a)). The target thickness of the argon was 4.5×10^{14} cm^{-2} so that at least one collision would be expected to occur on the average. (Target thickness is defined as the target density integrated along the axis of the

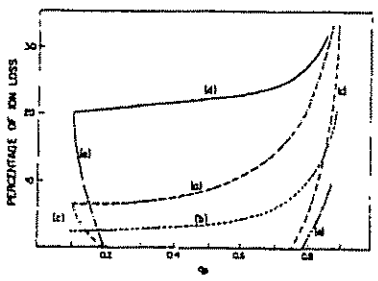

Fig. 9. Calculations of the percentages of stored ions that would be lost for changes in a transverse velocity caused by gas scattering in QUAD 2. (a) A 50% reduction in velocity, occupied $\epsilon = \epsilon_{max}$. (b) a 25% reduction in velocity, occupied $\epsilon = \epsilon_{max}$. (c) a 25% reduction in velocity, occupied $\epsilon = \epsilon_{0.1}$; (d) a 25% increase in velocity, occupied $\epsilon = \epsilon_{max}$; (e) a 25% increase in velocity, occupied $\epsilon = \epsilon_{0.1}$.

central quadrupole.) The only process likely to occur other than scattering losses is electron detachment. For O^- at 55 eV, the cross-section has been measured [20] as 6×10^{-18} cm^2 and a detachment loss of O^- under the conditions of the experiment of 24% would be predicted. When q is not near the stability limits, the measured loss was 34%, so that the extra 10% would be the maximum loss due to scattering effects. The increased losses above q =

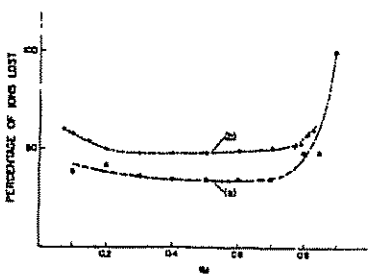

Fig. 10 Measurements of the percentage of ion loss versus q. Most of the losses can be accounted for by collision induced transitions. (a) O^- ions at 55 eV laboratory energy colliding with argon at a target thickness of 4.5×10^{14} cm^{-2}. (b) $C_2H_5OH_2^+$ ions at 5 eV laboratory energy colliding with methane at a target thickness of 4.6×10^{14} cm^{-2}.

0.8 are expected from the theoretical modelling. For experiments involving I^-, the loss averaged about 17% under similar conditions when $0.3 < q < 0.7$.

Curve (b) in Fig. 10 shows the loss of $C_2H_5OH_2^+$ ions in collision with CH_4 target gas at a thickness of 4.6×10^{14} cm^{-2} and a median laboratory energy of about 5 eV. The principal ion loss is by dissociation and can be accounted for by the number of observed daughter ions. The increases in ion loss at low and high q are presumably the result of scattering.

From these results and calculations, it can be seen that quantitative measurements of ion dissociation should be possible down to cross-sections of a few square angstroms. Further evidence of low ion loss by scattering comes from the total number of ions (parents plus daughters) observed as a function of target thickness. This is discussed in the concluding section, after daughter containment has been considered.

THE CONTAINMENT OF DAUGHTER IONS

When a parent ion dissociates into a daughter ion, there is a sudden change in q given by $q_d = q_p M_p / M_d$. Such a change can lead to daughter ion loss, if the daughter u, $\dot{u}$ value lies outside the new acceptance ellipse. Recent measurements [7—10] have shown that daughter ions often have approximately the same velocities after collision as the parent ion. As a simple approximation, it is assumed here that the internal energy transfer can be neglected so that the transverse velocity remains constant. The effect of the sudden change in q will again depend upon the phase of the r.f. field at the moment of dissociation. Consider a parent with $q_p = 0.1$. At the zero phase, when the acceptance ellipse is oriented along the u axis, the daughter ions will always be contained provided $\epsilon_{daughter} > \epsilon_{parent}$, which Fig. 3 shows to be valid for daughters up to $q = 0.895$. However at some other phase, the orientation of the daughter acceptance ellipse in the phase plane will be different from that of the parent and the two ellipses will not overlap completely. The ellipse overlap has been calculated and averaged for twenty different initial field phases and the percentage of ions retained is plotted in Fig. 11, taking into account the two coordinate directions and assuming $q_p = 0.1$. The loss of daughter ions can be quite significant when the parent acceptance ellipse is uniformly occupied (curve (a)). However, the losses arise mainly from ions with large u values at the moment of dissociation. If the parent acceptance ellipse area is only one-quarter occupied (curve (b)) there is little loss of ions with $q_d > 0.6$. In the constant q daughter mode of scanning q_d can be selected in order to avoid losses due to the transformation in q. The results are very similar for other q_p values. The theoretical calculations explain the observations of Fig. 5 that daughter ions are not well retained when $q_d > 0.7$. QUAD 2 had been tested separately for ion storage as a stand-alone quadrupole and was found to behave normally with a limit to ion containment near $q = 0.91$.

208

Fig. 11. Calculations of the retention of daughter ions after their formation from a parent at $q_0 = 0.1$. Curve (a) assumes the parent acceptance ellipses to be uniformly occupied and curve (b) assumes that the parent acceptance ellipses are only one-quarter occupied.

THE PATH LENGTH OF PARENT IONS

From the exponential decline of parent ion intensity with target thickness [6–10] (see Fig. 12 for example), the nominal total cross-section for

Fig. 12. Measurements of ion intensity versus target thickness for $H(H_2O)_3^+$ dissociation on collision with argon to $H(H_2O)_2^+$ and H_3O^+.

209

ion loss can be calculated readily. However, the target thickness has generally been calculated on the basis of the axial path length of the parent in QUAD 2. The actual path length, including the transverse oscillations is greater so that cross-sections have been overestimated. Based on the filling of the acceptance ellipses reported here (Fig. 5) the order of magnitude of the necessary correction can be calculated. This is most easily examined using some already published values of the transverse velocity distributions [21]. The average transverse velocity is a function of the phase of the r.f. field. Values for the root mean square velocity have been calculated for $a = 0$ and $q = 0.86$, 0.64 and 0.28 for full occupancy of the phase space acceptance ellipses. The average transverse velocity in each direction is 0.85 times the root mean square velocity. At the lowest q values (0.28), the velocity is not a strong function of the field phase and a mean overall value of 0.085r_0/ξ can reasonably be assumed where $\xi = \omega t/2$.

Taking the actual velocity as $(v_x^2 + v_y^2 + v_z^2)^{0.5}$ and calculating the ratio (R) of the real distance travelled versus the axial distance as $R = (1 + (v_x^2 + v_y^2)/v_z^2)^{0.5}$, one obtains

$$R = (1 + 0.0736 r_0^2 FM/E)^{0.5}$$

where r_0 is in centimetres, F is the frequency in megahertz, M is the ion mass in amu and E is the axial energy in electronvolts. Thus, for this instrument where $r_0 = 0.873$ cm and $F = 1.13$, a ratio M/E of unity gives a path length correction of only 2%. Ions with a ratio of M/E of 10 will give a correction factor of 20%. These calculations are based on operation at $a = 0$, $q = 0.28$ with full uniform occupation of the acceptance. If the source emittance only fills the acceptance at $q = 0.1$ as indicated in Fig. 8, then the acceptance at $q = 0.28$ is only about one-quarter occupied, the mean transverse velocity is correspondingly reduced and the path length correction factor is small. For this instrument, it is concluded that the measurements of cross-section for ion loss should be quite reliable.

SUMMARY AND DISCUSSION

The containment of ions in an r.f. only quadrupole field as used in triple quadrupoles for collision induced dissociation of ions, has been examined experimentally and theoretically. The choice of operating conditions for the collection of standard spectra, and for obtaining quantitative data on ion dissociation, has been considered with specific reference to the following four points:

(1) the dependence of storage of the parent ion on the r.f. voltage (i.e. upon q_0);

(2) the susceptibility of ions to loss by gas scattering and its dependence on q_0;

(3) the ease of ions likely to arise from the sudden transformation in mass

caused by fragmentation to daughter ions;

(4) the actual average path length of the parent ions compared to the nominal path length in QUAD 2.

In all cases, the theoretical model of ion containment is in good agreement with the experimental data. The choice of the operating mode of QUAD 2 is important in deciding the relative intensities of different parts of the daughter ion spectrum. It is suggested that the 'constant q daughter' operating mode, where $(r.f.)_2$ is kept in constant ratio with $(r.f.)_3$ throughout a scan, has many advantages for general purpose analysis. The 'constant q parent' operating mode is more appropriate for examining ion/molecule addition products.

The theory and the experiments indicate that a very low loss of ions can be achieved under well-chosen conditions. The experiments were performed in a system where there is very efficient coupling between the various quadrupoles and ions never leave the quadrupole field. In instruments where the three quadrupole fields are isolated from each other, the effects of exiting and re-entering through fringing fields would have to be taken into account. Obviously when restrictive apertures are placed between the quadrupoles, transmission is likely to be limited and ion scattering is more likely to lead to ion loss. Another complication arising from the presence of interquad restrictions is the occurrence of focusing and defocusing effects at the exit of QUAD 2. These effects are axial velocity dependent and also depend upon the choice of r.f. voltage. In the constant q daughter mode of scanning, with a suitable choice of $(r.f.)_2/(r.f.)_3$, the principal effects can certainly be avoided if any interquad aperture has a diameter greater than $1.4r_0$.

In the triple quadrupole described here, it was concluded that the loss of ions due to gas scattering is very small when operating conditions are carefully chosen and that daughter ions can be captured with very high efficiency so that quantitative measurements can be made. This has been supported in three detailed studies [7,9,10] of the kinetics of ion dissociation for some very different ions, e.g. $C_6H_5Br^+$, the protonated parent ion of a phosphorus ester (DMMPA) of mass 196 and the water clusters $(H_2O)_2H^+$ and $(H_2O)_3H^+$. In each case, the loss of parent ions was accounted for by the appearance of daughter ions at least up to a target thickness of about 7×10^{14} cm^{-2}. To illustrate this point further, Fig. 12 shows the curves for the declustering of $(H_2O)_3H^+$ as a function of target thickness. These results were undertaken under conditions where the parent transmission was constant (see Fig. 8) during measurement of the daughter ions. The total number of ions remained essentially constant despite the presence of the argon in QUAD 2 and the transformation in ion mass (and therefore in q) on dissociation. At higher target thicknesses, significant H^+ formation is predicted and this ion was not directly observable. These various measurements present persuasive evidence that, under well-chosen conditions in an instrument of good design, almost all the daughter ions can be collected, regardless of scattering angle, and that total cross-sections for dissociation can be measured. However, this only applied if QUAD 3 is operated under conditions which are non-discriminatory with mass. This is true, for example, when QUAD 3 is operated under source limited conditions (the source being ions from QUAD 2). Alternatively QUAD 3 should be operated with an a/q ratio which is kept constant with mass. Many conventional commercial quadrupole power supplies are designed [13] with an a/q ratio which increases with mass and these would introduce discrimination against higher mass ions.

ACKNOWLEDGEMENTS

We would like to express our gratitude to D.J. Douglas, J.A. Buckley and J.B. French for helpful discussions.

REFERENCES

1 R.A. Yost and C.G. Enke, J. Am. Chem. Soc., 100 (1978) 2274.
2 R.A. Yost, C.G. Enke, E. McGilvery, D Smith and J.D. Morrison, Int. J. Mass Spectrom. Ion Phys., 30 (1979) 127.
3 D.F. Hunt, J. Shabanowitz and A.B. Giordani, Anal. Chem., 52 (1980) 386.
4 D. Zakett and R.G Cooks, Anal. Chim. Acta, 119 (1980) 129.
5 J.A. Buckley, D.J. Douglas, D. Simmons, P.H. Dawson and J.B. French, Proc. 1981 Pittsburgh Conf. on Analytical Chemistry and Applied Spectroscopy.
6 P H. Dawson, J.B. French, J.A. Buckley and D Simmons, Org. Mass Spectrom., (1982) in press.
7 P.H. Dawson, J.B French, J A Buckley, D.J Douglas and D Simmons, Org Mass Spectrom., (1982) in press
8 P.H. Dawson, J.B French, J.A. Buckley and D. Simmons, 29th Ann. Conf on Mass Spectrometry, Minneapolis, MN, 1981.
9 D J. Douglas, J. Phys. Chem., (1982) in press.
10 P.H. Dawson and D.J. Douglas, Proc 29th Ann Conf. on Mass Spectrometry, Minneapolis, MN, 1981.
11 TAGA 6000, Sciex Inc., 55 Glen Cameron Road, Thornhill, Ont. L3T 1P2, Canada
12 P.H. Dawson, in C. Marton (Ed.), Advances in Electronics and Electron Physics, Vol. 53, Academic Press, New York, 1980.
13 P.H. Dawson, Quadrupole Mass Spectrometry and its Applications, Elsevier, Amsterdam, 1976.
14 P.H. Dawson, in A. Septier (Ed.), Advances in Electronics and Electron Physics, Suppl. 13B, Academic Press, New York, 1980.
15 P.H. Dawson, J.B. French and J A. Buckley, to be published.
16 R.F. Lever, IBM J. Res. Develop., 10 (1966) 53
17 P H. Dawson, Int. J. Mass Spectrom. Ion Phys., 21 (1976) 317.
18 D.M. Mintz, C.A. Boltnott and U. Steiner, Proc 29th Ann. Conf. on Mass Spectrometry, Minneapolis, MN, 1981.
19 P H. Dawson, Int. J. Mass Spectrom. Ion Phys., 24 (1977) 447.
20 H.S.W. Massey and H.B. Gilbody, Electronic and Ionic Impact Phenomena, Oxford University Press, Oxford, 1974
21 P.H Dawson, Int. J. Mass Spectrom Ion Phys., 20 (1976) 237.

R. A. Yost
Department of Chemistry
University of Florida
Gainesville, Fla. 32611

C. G. Enke
Department of Chemistry
Michigan State University
East Lansing, Mich. 48824

Triple Quadrupole Mass Spectrometry for Direct Mixture Analysis and Structure Elucidation

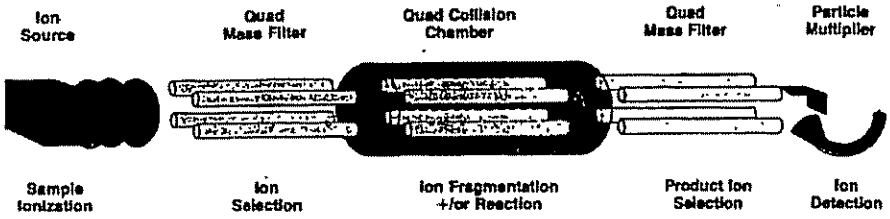

Figure 1. Conceptual diagram of the triple quadrupole mass spectrometer showing each component and its function

A new technique of mass spectrometry is rapidly emerging in which tandem mass analyzers are used for separation and identification in a single instrument. In this technique (MS/MS), several ionic species are generated from a sample; ions of a particular mass are selected for fragmentation; the selected ions are fragmented by one of several possible techniques; and the resulting fragment ions are mass-analyzed. We recently introduced the concept of a triple quadrupole mass spectrometer as a particularly simple and efficient approach to selected ion fragmentation (1). The instrument consists of, in series, a dual chemical ionization/electron impact (CI/EI) sample ionization source, a quadrupole mass filter, an RF-only quadrupole that can be pressurized with a collision gas, a second quadrupole mass filter and an electron multiplier, as shown in Figure 1. The ion fragmentation process is performed by collision-induced dissociation (CID) in which the ion acquires internal energy by collision with a neutral molecule. The RF-only quadrupole collision chamber provides focusing of scattered ions and is highly efficient (2). In this system, the selected ion fragmentation process can provide enhanced selectivity and discrimination over normal mass spectrometry without significant loss of sensitivity.

An Added Dimension of Information

The added information contained in the fragmentation spectrum of each source ion species is of great value in several areas of mass spectrometry, especially the elucidation of organic structures and the analysis of mixtures. In structure elucidation applications, fragment ions of any mass which appear in a compound's normal mass spectrum can be selected with the first mass analyzer. This parent ion is further fragmented, and the mass spectrum of the resulting daughter ions is determined by scanning the second mass analyzer. A complete fragmentation map may be obtained by recording the mass spectrum of each fragment ion of a compound. Figure 2 is an example of such a map for cyclohexene. Note that the normal electron impact mass spectrum, displayed along the diagonal (fragment ion m/z = parent ion m/z), is the only information available without the added dimension of selected ion fragmentation.

For analysis of mixtures, the molecular ions for each component can be

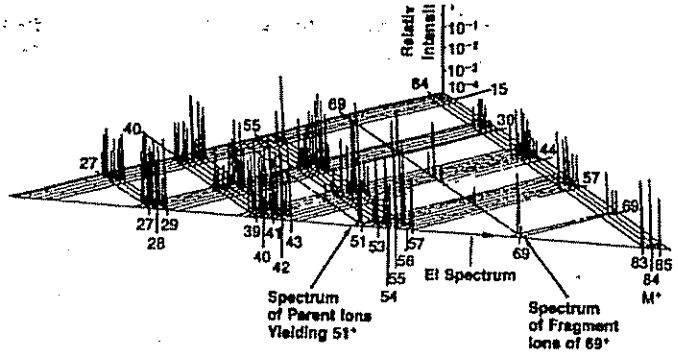

Figure 2. Three-dimensional fragmentation map for cyclohexane

produced by soft ionization such as chemical ionization or field desorption and then separated by the first mass analyzer. Thus the molecular ion species can be selected for one component at a time, the selected ion fragmented, and its fragmentation mass spectrum obtained by scanning the second analyzer. The added dimension in this case is the selectivity and discrimination achieved through mass separation of the molecular ions of the several components. The elimination of chemical noise that results can often improve the detection limit of the mass spectral technique (*3*).

The use of mass spectral separation of the components of a mixture in MS/MS eliminates the time delays associated with the chromatographic separation used in GC/MS and LC/MS. Because all the components are available at any time and in any order, only those components of particular interest need be analyzed. Each component may be selected for as much or as little time as is required to determine its identity and its quantity. Continuous analysis of a sample is possible in such applications as atmospheric analysis, without the time delays associated with batch sampling for chromatographic analysis. Direct insertion probes and field or chemical desorption can be used to introduce involatile or thermally labile samples.

Other Selected Ion Fragmentation and Tandem Mass Spectrometers

There are several other approaches to selected ion fragmentation, the most notable of which for analytical applications is Mass-Analyzed Ion Kinetic Energy Spectrometry, or MIKES (also called Collisional Activation Mass Spectrometry or CAMS, and Direct Analysis of Daughter Ions or DADI). This technique makes use of a double-focusing mass spectrometer in which the magnetic sector precedes the electrostatic analyzer. Fragmentation between the sectors can be unimolecular (metastable ions) or collisionally induced. MIKES has been demonstrated as a technique for selected ion fragmentation in such applications as structure elucidation (*4–8*) and mixture analysis (*3, 9*). The structure elucidation technique has been clearly described by Beynon (*8*). The technique for analysis of mixtures has been reviewed by Cooks in these pages (*3*). It is also possible to emulate the MIKES technique with a normal geometry double-focusing mass spectrometer (electric sector preceding the magnet) and a linked scan of both the electric sector field strength and either the magnetic field or accelerating voltage (*10*). Ions enter the CID collision chamber in sector instruments with 3-30 keV of kinetic energy. The mechanism of the CID process at these high energies is fundamentally different from the process at the low kinetic energies (3-50 eV) of ions in the triple quadrupole instrument (*11*).

True tandem mass spectrometers have been constructed to apply selected ion fragmentation techniques to the study of interactions between ions and molecules (*12*). Two quadrupoles in tandem have been employed to study ion-molecule reactions (*13*), and triple quadrupole systems have been applied to study the photodissociation of ions (*14, 15*). However, it is the low-energy CID process in the center quad that makes the triple quadrupole spectrometer described here particularly well suited for analytical applications. Hunt and co-workers have recently reported on the analytical applications of a triple quadrupole instrument constructed in their laboratory (*16*).

Modes of Operation

There are three fundamental control parameters in the triple quadrupole mass spectrometer. These are the mass selected by the first mass analyzer, the presence or absence of collision gas in the quad collision chamber, and the mass selected by the second mass analyzer. These parameters may all be varied independently or in combinations to provide a variety of useful modes of operation as enumerated and described below:

- In order to obtain a normal mass spectrum (only one stage of mass analysis), the first mass filter is scanned with the second and third quadrupoles in RF-only (total-ion) mode. The collision gas may be present or not, since it does not significantly affect the number of ions reaching the detector.
- A scan of the third quadrupole while the first mass filter passes a specific mass produces a spectrum of all the daughter ions from the selected parent ion. If the collision gas is absent, the unimolecular decomposition products ("metastable" ion decomposition) will be measured.
- The spectrum of all parent ions that fragment to produce a given daughter ion is observed by scanning the first mass filter with the third quadrupole fixed on the daughter ion mass.
- The observation of a specific neutral mass loss is achieved by scanning both mass filters with a fixed difference in mass. The use of a double-focusing mass spectrometer for neutral loss spectra has been suggested recently as a useful but complicated technique for structure elucidation (*17*).
- A specific parent/daughter ion transition is selected in single reaction monitoring (*18*), a technique analogous to single ion monitoring in gas chromatography/mass spectrometry.
- The quadrupole's linear mass scale and fast response permit rapid multiple reaction monitoring in which multiple parent/daughter ion pairs are observed.

Mixture Analysis

As an example of the performance of the triple quadrupole mass spectrometer, the following sample which contains five components at equal concentration was chosen: 3-heptanone and *n*-heptanal (isomers of molecular weight 114), *n*-octane (isobaric with the other two at 114), cyclohexane (84), and 2-pentanone (86). The mixture was ionized by 70 eV EI, although CI would have simplified the mass spectrum. The CID spectra of the 114^+ ion from the individual components show unique fragmentation: 99^+ (M-15) for 3-heptanone, 96^+ (M-18) for *n*-heptanal, and 70^+ ($C_5H_{10}^{+\cdot}$) for *n*-octane. In the CID spectrum of the 114^+ ion in the mixture, it is possible to detect the individual compo-

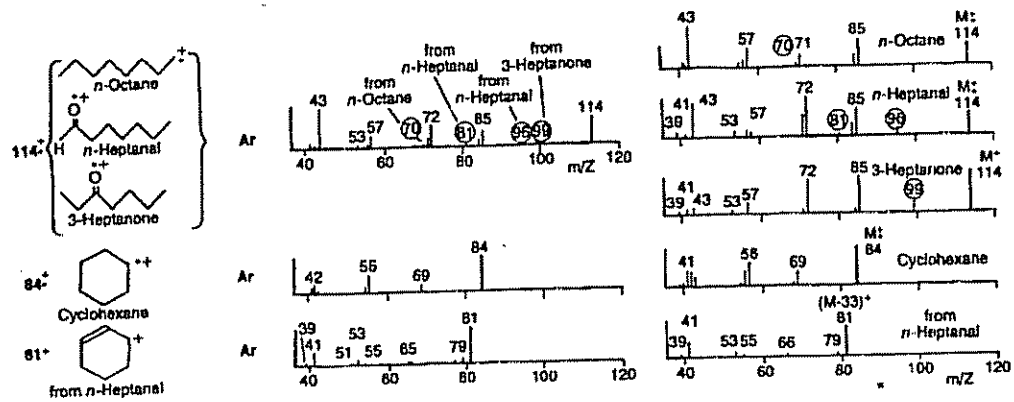

Figure 3. Comparison of CID spectra of selected ions in the EI spectrum of a five component mixture with reference CID spectra from pure components

nents despite their being isomeric or isobaric. Figure 3 shows the CID spectrum of the 114^+ ion in the mixture as well as the reference CID spectra of 114^+ from the three pure compounds. The two isomers in the mixture may be identified with even greater confidence by obtaining the CID spectra of fragment ions produced by EI that are unique to the specific components. The CID spectra of 99^+ and 81^+ from the mixture exactly match the spectra of the 99^+ fragment from pure 3-heptanone and the 81^+ fragment from *n*-heptanal, respectively. The other two components are most readily identified in the mixture; the CID spectra of the molecular ions of pure cyclohexane (84^+) and 2-pentanone (86^+) are nearly perfect matches with the CID spectra of these ions from the mixture. The CID spectra obtained for 84^+ and 81^+ from the mixture are compared with reference spectra in Figure 3.

A sixth and unexpected component was discovered and identified in the mixture as well. The electron impact spectrum showed peaks at 120^+ and 105^+ which could not be attributed to any of the five known components. The CID spectra showed fragments from 120^+ at 105^+, 43^+, and 77^+, and fragments from 105^+ at 77^+, 51^+ and 26^+. Interpretation of these data suggested acetophenone as the impurity, and a comparison with the reference CID spectra of 120^+ and 105^+ ions from pure acetophenone confirmed this. Careful study of the EI spectra of the individual components showed that the acetophenone was present as an impurity in the *n*-heptanal. A single standard addition experiment indicated an acetophenone concentration of approximately 5 parts per 1000 in the *n*-heptanal and therefore 1 part per 1000 in the mixture. These results demonstrate the ability of the triple quadrupole system to identify mixture components, including both isomers and isobaric compounds. The high sensitivity of the system for trace analysis is discussed in the instrument performance section.

Structure Elucidation

As an example of a structure elucidation application, consider unknown 5.13 in McLafferty's classic text (*19*) on mass spectral interpretation. The EI spectrum shows molecular weight 120 with major peaks at 105 and 77. Considering the 77 peak (phenyl moiety) and 105 (loss of methyl), there are two possible compounds, $C_6H_5COCH_3$ and $C_6H_5CH(CH_3)_2$. Relying on the 121/120 ratio and the unusually small hydrogen-loss ions from 120 and 105, McLafferty concludes that the unknown is acetophenone, $C_6H_5COCH_3$. The structure of this unknown can be obtained in a direct manner using selected ion fragmentation on the triple quadrupole mass spectrometer. The large 43^+ peak in the EI spectrum corresponds to the remainder of the molecule [CH_3CO^+ or $(CH_3)_2CH^+$] after loss of 77 (C_6H_5). The CID spectrum of 43^+ is shown in Figure 4. Interpretation of the data indicates the fragmentations shown for CH_3CO^+. The reference CID spectra of known ions shown in Figure 4 confirm that 43^+ from acetophenone matches the CID spectrum of CH_3CO^+ from acetone, but is significantly different from that of $(CH_3)_2CH^+$ from cyclohexane. Thus, McLafferty's conclusion is confirmed. The process of structure elucidation of this unknown has been made simpler and more reliable by the added information available by selected ion fragmentation.

Ultimately, the formation and fragmentation of every ion in a com-

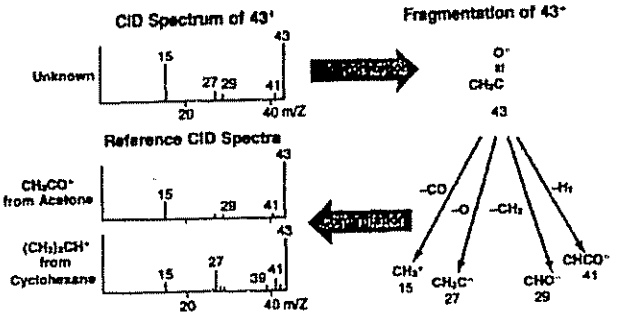

Figure 4. Structure elucidation of 43^+ functional moiety by interpretation of CID spectrum and comparison with reference CID spectra

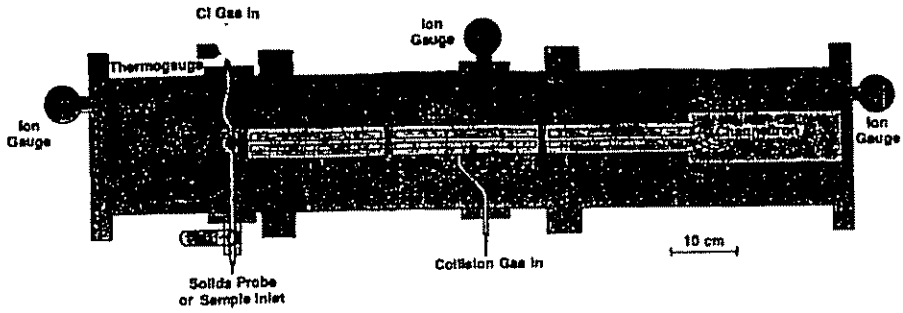

Figure 5. Scale drawing (top view) of triple quadrupole mass spectrometer

pound's mass spectrum may be determined to yield a complete map of the fragmentation pathways for the molecule. Such a map, for cyclohexane, appears in Figure 2. This approach has been employed in a detailed study of the fragmentation of nonan-4-one (20). In that study, over 400 distinct collision-induced fragmentations have been observed, a tenfold increase over the number previously observed in metastable studies (21). These include a number of new fragmentations of very low intensity such as loss of water from the α-cleavage ions. The high sensitivity of the triple quadrupole instrument has made it possible to observe these transitions.

Description of Instrument

A scale drawing of the triple quadrupole spectrometer constructed at Michigan State University appears in Figure 5. The path length from source to detector is approximately 67 cm. The individual components of the system, including the source, quadrupoles, detector, vacuum system, and control electronics, are described below.

Samples may be introduced through a heated glass inlet system or a heated direct-insertion probe. The ion source is a Finnigan CI/EI model 3000. The first quadrupole mass filter is a standard Extranuclear Labs ELFS model with 0.95 cm diameter × 20 cm long rods and a mass range of 1-1000 amu. The center quadrupole is a homemade model with 0.954 cm diameter × 21.6 cm long stainless steel rods. Flat plate lenses on each end of the center quadrupole aid in focusing the ion beam between quadrupoles. Another Extranuclear mass filter serves as the third quadrupole. It is identical to the first except that the small (0.2 cm diameter) entrance aperture has been removed. The axial ion energy in the three quadrupoles may be varied independently over the range −100 to +100 V, with −10 V being typical for positive ions. The positive ions are detected with a Galileo 4770 high-current Channeltron with a measured gain of 3×10^6 at −3 kV. The current from the multiplier is detected with a Keithley 18000-20 picoammeter with programmable ranges of 10 V/10^{-10} A to 10 V/10^{-3} A.

The components of the mass spectrometer are enclosed in three differentially pumped stainless steel chambers, each pumped by an oil diffusion pump with water-cooled baffle (Figure 5). Normal operating pressures in the three chambers, as indicated by ion gauges, are source chamber: 2×10^{-7} torr for EI and 6×10^{-4} torr for CI; center chamber: 2×10^{-5} torr (no collision gas); detector chamber: 2×10^{-6} torr. Collision gas pressures from 2×10^{-4} torr to 1×10^{-2} torr are possible.

The entire vacuum system is interlocked to provide fail-safe operation and permit computerized cycling of the vacuum system. Foreline pressures, coolant water flow, electric current through the pumps, pneumatic pressure, and valve positions are all monitored and used to control the proper sequencing of all pumps, electropneumatic valves, and electronics.

Data acquisition from the system is currently either manual (strip chart recorder or oscilloscope), or automated with an Intel SDK-85 microprocessor, CRT terminal, and floppy disc. A multiple microprocessor system employing the Intel 8085 is currently under development for data acquisition and intelligent control of the instrument. The entire system has been designed for computer control, including the mass selection in both mass filters, the selection of mass filter or total-ion mode, the RF voltage on all three quadrupoles, the control of collision and CI gases, and the vacuum interlock. The capabilities of the triple quadrupole system for selected ion fragmentation will be significantly enhanced under complete computer control.

Performance of Instrument

The use of quadrupoles as mass filters and as the CID chamber has provided the anticipated excellent selectivity and sensitivity. Selectivity is achieved by tandem mass separation up to mass 1000 with a resolution of better than 1 amu. The high sensitivity (detection limit of 10^{-15} mole) results from the very efficient low-energy CID process and the high transmission of each component along the ion path.

Resolution. The ultimate resolution of the quadrupoles is approximately 1 part in 1500, as determined by measuring peak width at half height. As an example of the resolving power, the N^+-/CH_2^+- doublet at 14 amu can be resolved (50% valley) which requires a resolution of 1 part in 1100. The mass filters can be operated in two modes: constant resolution and resolution proportional to mass. At constant resolution (e.g., 1 part in 1000 over entire mass range) the relative abundance of the ions in a mass spectrum closely resembles that observed with magnetic mass spectrometers. With resolution proportional to mass (e.g., 1 part in 100 at mass 50, 1 part in 1000 at mass 500), the intensity of the low mass peaks is enhanced. The quadrupoles are typically operated with unit mass resolution (1% valley) over the entire mass range. The peak broadening due to kinetic energy loss on fragmentation that is observed with MIKES instruments does not occur with the quadrupole mass filter.

CID Efficiency. The high sensitivity of the triple quadrupole system is a result of the high efficiency of each component. The ion source and lenses produce approximately 1 ion for every 2×10^5 molecules. The mass filters have a transmission efficiency of approximately 60% in RF-only mode and 10% in mass filter mode with resolution of 1 part in 200. The center qua-

quadrupole has virtually 100% transmission. Even more important is the efficiency of the CID process which occurs in the center quadrupole. In an earlier investigation of the low-energy CID process in a triple quadrupole system (2), three expressions were developed to describe the efficiency. The collection efficiency is the ratio of the ion flux at the exit of the quadrupole to that at the entrance. With no collision gas present, there is 100% collection. At 2×10^{-4} torr collision gas pressure, the collection efficiency ranges from 50% for light ions like CH_4^+ up to 75% for heavier ions which are less prone to scatter. The strong focusing of the quadrupole field minimizes scattering losses. The fragmentation efficiency is the fraction of the ion flux at the exit of the center quad that is due to fragment ions. At 2×10^{-4} torr, fragmentation efficiency ranges from 15% to 65% for various compounds (2). As the collision gas pressure is increased, the fragmentation efficiency for all compounds approaches 100% due to multiple collisions, but the collection efficiency decreases due to scattering. The overall CID efficiency, which is the product of the collection and fragmentation efficiencies, exhibits a maximum at some intermediate pressure. The collection efficiency as a function of collision gas pressure for the dissociation of CH_4^+ from methane is shown in Figure 6. The fragmentation efficiences for the production of the CH_3^+ and CH_2^+ ions are also shown.

Several factors other than collision gas pressure can affect the efficiency of the CID process (2). The larger the molecular diameter of the collision gas, the more efficient the CID. Ion axial energy and ion internal energy also affect the CID process. A more detailed study of these effects is in progress (*11*).

Sensitivity. The overall sensitivity of the instrument can be estimated from the product of the efficiencies of the individual processes. The source efficiency and the transmission through the three quads (without collision) are 2×10^{-5} and 10^{-2} respectively. The fragmentation efficiency is a function of the ion and fragment selected, but from Figure 6 it is seen to be about 0.1 for $CH_4^+ \rightarrow CH_3^+$. The overall efficiency is 2×10^{-8}, that is, two CH_3^+ ions reach the detector per 10^8 CH_4 molecules passing through the source. The detection system can measure the current due to one ion per sec which is an average current of 5×10^{-19} A. For methane, then, a current of 4×10^{-10} A will be produced from a sample flux of 1 pg per sec.

The ultimate detection limit depends on the system sensitivity, the

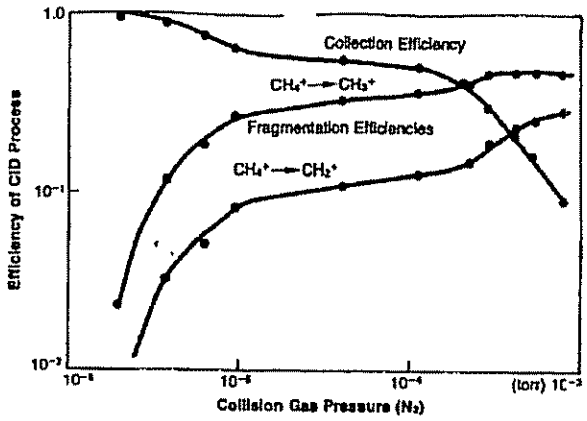

Figure 6. Effect of collision gas (N_2) pressure on CID efficiency for methane $CH_4^{+\cdot}$ at ion axial energy of 10eV

chemical and electrical noise levels, and the lowest measurable signal level. The electrical noise in the system is typically 3×10^{-13} A. The two stages of mass separation often make it possible to reduce chemical noise (ions detected from other than the desired reaction) to well below the 10^{-13} A level. In such a case, at the extreme sensitivity limit, the peak height is quantized by the integer number of ions which reach the detector during the scanning time of the peak. The detection of 4 ions would give an S/N of 2 and, for methane, would require 6 fg of sample. The detection limit for methane has been determined experimentally to be 16 femtograms by measuring a sample of 10 ppm CH_4 in N_2 at a sample flux of 20 femtograms per sec of CH_4. The large excess of N_2 is required to increase the ion source pressure so that it can be accurately measured and the sample flux calculated. The selectivity of monitoring the $CH_4^{+\cdot} \rightarrow CH_3^+$ reaction has effected a two order of magnitude improvement in detection limit compared to that obtained by simply monitoring the $CH_4^{+\cdot}$, CH_3^+, or $CH_2^{+\cdot}$ ions from electron impact. This improvement is due to the elimination of the chemical noise introduced by background $^{14}N^{+\cdot}$, $^{15}N^{+\cdot}$, and $^{16}O^{+\cdot}$ peaks.

The selected ion fragmentation capability of the instrument produces only a small loss in transmission and sensitivity, and produces a significant gain in selectivity. Indeed, in the normal case where the system is limited by chemical rather than electrical noise (3), a substantial improvement in detection limit can be achieved as was observed for methane. The detection limit of approximately 10^{-15} mole is made possible by the high efficiency of every component of the system.

The detection limit for a higher mass organic compound, nitrobenzene, has also been determined experimentally. The transition $NO_2C_6H_5^{+\cdot} \rightarrow C_6H_5^+$ was monitored at unit mass resolution in both mass filters, with the parent ion produced by electron impact on a sample of 10 ppm nitrobenzene in N_2. A detection limit of 120 femtograms (S/N = 2) was obtained with a sample flux of 200 femtograms/sec. In comparison, for the MIKES technique, Cooks has estimated a detection limit of 10 pg for the $140^+ \rightarrow 123^+$ transition of protonated nitrophenol ions produced by CI (22). Although consumption of only femtograms is required for recording the single reaction, actual sample size is significantly larger than this and is dependent on the sample inlet used. Total consumption of a sample introduced by direct probe should make it possible to detect quantities of individual components at close to these detection limits.

Conclusions

The CID process performed in the strong focusing field of an RF-only quadrupole is efficient and effective in producing characteristic spectra of selected ions. The kinetic energy independence of the mass resolution is ideal for collision product analysis. The lack of interdependence in the control of the two mass filters makes

it easy to implement the various analytical modes.

The system can be used to detect species present in a mixture including isomers without prior separation at the 10^{-15} mole level. The capability to select a desired initial mass and specific collision product mass reduces chemical noise dramatically. For structure elucidation applications, the spectra of selected functional moieties in the molecule may be obtained. Among the many other promising applications of the selected ion fragmentation technique is the analysis of isotopically labeled samples, in which the first mass filter can eliminate interferences from molecules that are not completely labeled.

Acknowledgment

We wish to acknowledge the work of the MSU Chemistry Department Machine Shop headed by Russ Geyer, and master machinist Len Eisele who constructed much of the instrument. We would also like to express our gratitude to Kaz Latven, John Chakel and Fritz Allen who helped to get the instrument functioning and to demonstrate its application. Finally, we would like to acknowledge the invaluable time spent in the laboratory of Jim Morrison at La Trobe University and helpful discussions with Graham Cooks and Chuck Sweeley.

References

(1) R. A. Yost and C. G. Enke, *J. Am. Chem. Soc.*, 100, 2274–75 (1978).
(2) R. A. Yost, C. G. Enke, D. C. McGilvery, D. Smith, and J. D. Morrison, *Int. J. Mass Spectrom. Ion Phys.*, 30, 127–136 (1979).
(3) R. W. Kondrat and R. G. Cooks, *Anal. Chem.*, 50, 81A–92A (1978).
(4) R. G. Cooks and J. H. Beynon, *MTP Int. Rev. Sci., Ser. II*, 5, 159 (1975).
(5) F. W. McLafferty, P. F. Bente, R. Kornfeld, S. C. Tsai, and T. Howe, *J. Am. Chem. Soc.*, 95, 3886 (1973).
(6) U. P. Schlunegger, *Angew. Chem. Int. Edn.*, 14, 679–88 (1975).
(7) K. Levsen and H. Schwarz, *Angew. Chem. Int. Edn.*, 15, 509–19 (1976).
(8) M. H. Bozorgzadeh, R. P. Morgan, and J. H. Beynon, *Analyst*, 103, 613–22 (1978).
(9) F. W. McLafferty and F. M. Bockhoff, *Anal. Chem.*, 50, 69–76 (1978).
(10) R. J. Strading, K. R. Jennings, and S. Evans, *Org. Mass Spectrom.*, 13 129–30 (1978).
(11) Manuscript in preparation.
(12) J. H. Futrell and T. O. Tiernan in "Ion-Molecule Reactions," J. L. Franklin, Ed., Chap. 11, Plenum, New York, 1972.
(13) T.-Y. Yu, M. H. Cheng, V. Kempter, and F. W. Lampe, *J. Phys. Chem.*, 76, 3321–30 (1972).
(14) M. L. Vestal and J. H. Futrell, *Chem. Phys. Lett.*, 28, 559–61 (1974).
(15) D. C. McGilvery and J. D. Morrison, *Int. J. Mass Spectrom. Ion Phys.*, 28, 81–92 (1978).
(16) D. F. Hunt and J. Shabanowitz, 27th Annual Conference on Mass Spectrometry and Allied Topics, Seattle, Wash., June 1979; paper FAMOC2.
(17) M. J. Lacey, C. G. MacDonald, *Anal. Chem.*, 51, 691–95 (1979).
(18) R. W. Kondrat, G. A. McClusky, and R. G. Cooks, *Anal. Chem.*, 50, 2017–21 (1978).
(19) F. W. McLafferty, "Interpretation of Mass Spectra," 2nd Ed., pp 95–6, W. A. Benjamin, Reading, Mass., 1973.
(20) Manuscript in preparation.
(21) G. Eadon, C. Djerassi, J. H. Beynon, and R. M. Caprioli, *Org. Mass Spectrom.*, 5, 917–33 (1971).
(22) T. L. Kruger, J. F. Litton, R. W. Kondrat, and R. G. Cooks, *Anal. Chem.*, 48, 2113–19 (1976).

This work was supported in part by the Office of Naval Research.

Chris Enke (left) and Rick Yost developed the triple quadrupole mass spectrometer at Michigan State University where Chris is professor of chemistry and Rick was a graduate fellow with support from the National Science Foundation and Analytical Division of ACS (sponsored by the Upjohn Company). Rick is currently assistant professor of chemistry at the University of Fla., Gainesville and is pursuing a research program in computer applications and modern instrumentation with special emphasis in mass spectrometry. The research program in Chris' lab at Michigan State University includes the development and application of computer-based instrumentation in optical spectroscopy, electroanalytical chemistry, and mass spectroscopy.

Fourier-Transform Electrospray Instrumentation for Tandem High-Resolution Mass Spectrometry of Large Molecules

Steven C. Beu, Michael W. Senko, John P. Quinn, Francis M. Wampler III, and Fred W. McLafferty
Department of Chemistry, Baker Laboratory, Cornell University, Ithaca, New York, USA

Mass spectrometry instrumentation providing unit resolution and 10-ppm mass accuracy for molecules larger than 10 kDa was first reported in 1991. This instrumentation has now been improved with a 6.2-T magnet replacing that of 2.8 T, a more efficient vacuum system, ion injection with controlled ion kinetic energies, accumulated ion trapping with an open-cylindrical ion cell, acquisition of 2M data points, and updated electrospray apparatus. The resulting capabilities include resolving power of 5×10^5 for a 29-kDa protein, less than 1-ppm mass measuring error, and dissociation of protein molecular ions to produce dozens of fragment ions whose exact masses can be identified from their mass-to-charge ratio values and isotopic peak spacing. (*J Am Soc Mass Spectrom 1993, 4, 557–565*)

Structural characterization by mass spectrometry is especially favorable for long-chain molecules, such as proteins, nucleotides, and carbohydrates, because backbone bond dissociation produces fragments whose masses are indicative of the structural units [1–3]. This has become an especially powerful routine method for oligopeptide sequencing [4, 5], even at the subpicomole level [6]. Of the 20 common amino acids of peptides/proteins, only leucine and isoleucine have identical masses, whereas the masses of lysine and glutamine differ by only 37 mDa. Complex mixtures of oligopeptides (< 3 kDa) can be routinely sequenced using a preliminary separation, such as by liquid chromatography, to yield fractions containing only a few oligopeptides. Tandem mass spectrometry (MS/MS, MS^n) can then separate molecular ions produced by soft ionization representing only one component of the mixture, with dissociation of these ions and MS-II analysis of the fragments to provide sequence information for the individual components [4–9]. Further dissociation of such fragment ions (such as $MS/MS/MS$) can then be used to distinguish Leu/Ile isobers [4, 5, 10] and provide confirmatory sequence information.

These same principles should apply to the structural characterization of even larger proteins and other long-chain molecules, but this requires a variety of improvements in techniques for ionization and ion dissociation and in instrumentation for resolution and mass measuring accuracy. Of revolutionary importance has been the development of several techniques for the ionization of large molecules, such as plasma desorption [11], fast-atom bombardment [12], matrix-assisted laser desorption [13] and electrospray ionization (ESI) [14–16]. For example, collisionally activated dissociation of singly charged oligopeptide ions has an upper limit of approximately 3 kDa [4, 5, 17]; ESI provides a very promising solution in that there appears to be no upper mass limit to the collisional dissociation of the multiply charged ions that it produces [18–20]. As a further advantage, the high number of charges of ESI ions of the highest mass values yields mass-to-charge ratio values generally in the range 500–2500, within the mass-to-charge upper limit of most types of mass spectrometers. This has the disadvantage, however, that the mass value must usually be derived from two or more peaks of the same mass value but different charge values; this becomes increasingly difficult for spectra containing an increasing number of mass values and/or decreasing number of charge values, such as the tandem mass spectrum from the dissociation of a large protein ion [19]. However, with unit resolution, the $^{12}C/^{13}C$ isotopic peaks provide a direct solution to this problem because the number of peaks in a mass-to-charge unit corresponds to the charge value [20–24].

Although magnetic sector instruments could achieve unit resolution for such large protein ions, the required narrow slits allow transmittance of only a concomitantly small proportion of the large mass range, which must be scanned while consuming the sample in continuous ionization. Array detectors [5] can measure a larger, but still relatively small, part of the spectrum with some sacrifice in resolving power. Further, these

Address correspondence to Fred W. McLafferty, Department of Chemistry, Baker Laboratory, Cornell University, Ithaca, NY 13853-1301

1044-0305/93/$6.00

Received January 28, 1993
Revised March 25, 1993
Accepted March 31, 1993

and most mass spectrometric instruments detect ions by collision with an electron multiplier; measuring ions nondestructively allows them to be remeasured for improved signal-to-noise ratio [25] and also to be dissociated or reacted for MS-II characterization [9], with this repeated for MS^n [26].

An instrument that appears to combine uniquely these attributes for MS^n of large molecules is the Fourier-transform ion cyclotron resonance (ICR) mass spectrometer [26–34]. Details are given here concerning an ESI Fourier-transform mass spectrometry (FTMS) instrument for the MS^n characterization of proteins that exhibits greater than 10^6 resolving power and less than 1-ppm mass measurement errors [20].

Experimental

The basic instrument configuration consists of a modified Millipore Extrel (Madison, WI) FTMS 2000 FT/ICR equipped with a 6.2-T magnet, an Odyssey data system, and external ESI source following the design of the earlier system [21–24]. The electrosprayed ions are conveyed from the source to the trapped-ion analyzer cell by three sequential radiofrequency-only quadrupole lenses through five stages of differential pumping (Figure 1).

The electrospray originates from a 32-gauge syringe needle biased at 2–3 kV, to which aqueous protein sample solutions are delivered at a flow rate of 1.5 μL/min by a Harvard Apparatus (South Natick, MA) syringe pump. The electrosprayed ions enter the first region of differential pumping through a 20-cm long, 0.5-mm inner diameter (i.d.) stainless steel capillary [35]. The capillary is resistively heated to temperatures of 100–250 °C, with applied direct currents of 2–6 A to promote desolvation of ions with no countercurrent gas flow [20, 24, 35]. The exit end of the capillary terminates 7 mm from a Beam Dynamics skimmer with a 0.5-mm sampling orifice (Minneapolis, MN); the capillary/skimmer region is evacuated to a pressure of 1 torr by a 38-L/s Laybold (Pittsburgh, PA) Sogevac SV280 rotary pump. Further desolvation of ions in this region is accomplished by collisional activation promoted by biasing the capillary at 150 V with respect to the skimmer, or higher potentials may be used to promote ion dissociation [18, 19].

Ions exit the skimmer (which is biased at 30 V relative to ground) and are conveyed into the Fourier-transform mass spectrometer by the three quadrupole lenses. Each quadrupole is independently evacuated, and conductance limits are located at the exit of each lens to provide three additional stages of differential pumping. Source isolation is provided by a 2.75-in. gate valve located between the first and second quadrupole, allowing source maintenance without venting the high-vacuum regions of the instrument. The first quadrupole is pumped by an 800-L/s Edwards diffusion pump (West Sussex, UK) to a pressure of 10^{-5} torr, the second by a 300-L/s Alcatel diffusion pump (Grand Island, NY) to 10^{-6} torr, and the third by a 1500-L/s Cryo-Torr model 8 cryopump (Helix Technology, Waltham, MA) to 10^{-8} torr. Two Extranu-

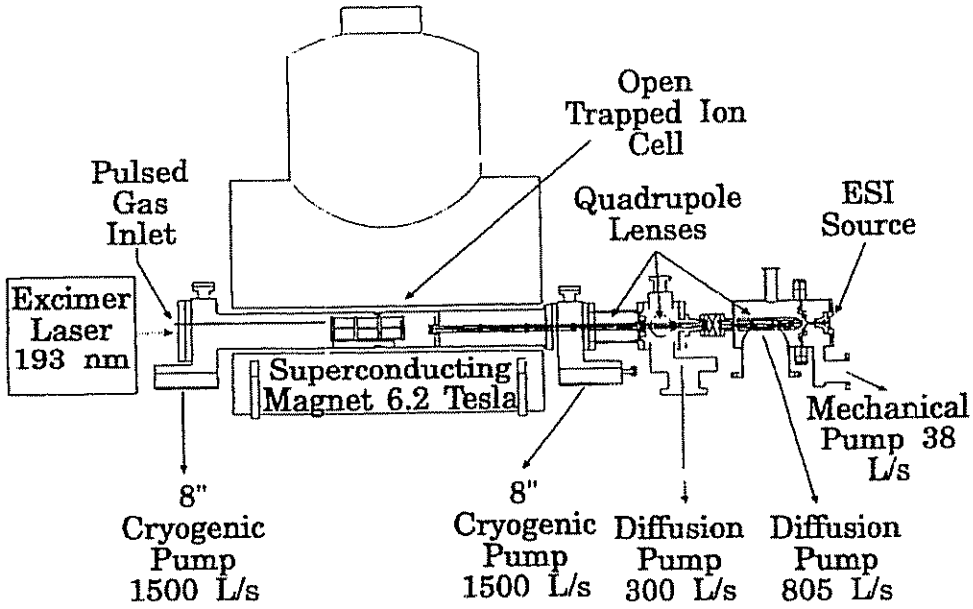

Figure 1. Schematic of new FTMS instrument.

TA 116

T005884

clear power supplies (Pittsburgh, PA) equipped with High Q heads drive the first quadrupole and the second and third quadrupoles in tandem, respectively. The first driver runs continuously, whereas the second is gated on by the data system only during ion injection events. Each driver may be independently biased to provide acceleration of ions between quadrupoles, with the first and second typically biased at 10–20 and −250 V, respectively. The first potential controls the final energy of ions entering the trapped-ion cell because this intralens region is the first in which the pressure is low enough for the ions to gain energy corresponding to the full potential drop between stages. The second potential provides high-energy injection of the ions for efficient penetration of the magnetic field; energy gained in this stage is lost when the ions exit the third lens, and thus its potential has little effect on the final energy of the ions.

Ions exit the third quadrupole well inside the high-field region of the magnet and travel a distance of 10 cm to the trapped-ion cell. Typical ion currents to the cell are 30–150 pA. The cell is an all-copper open cell [36] of cylindrical geometry (5-cm diameter) and a 2:1 aspect ratio. The cell region is evacuated with a second Cryo-Torr model 8 cryopump to provide the fifth and final stage of pumping. Base pressure in the analyzer region is typically less than 2×10^{-9} torr, with no measurable increase in pressure during operation of the external ESI source. Static trapping potentials are maintained during ion injection, and pulsed-valve introduction of nitrogen is used to effect collisional deceleration and retention of ions [22–24]. Because the pulse valves would not operate properly in the strong magnetic field, they are placed approximately 70 cm from the bore of the magnet, and a 3/8-in. o.d. stainless steel tube is used to conduct the gas to within 2 cm of the trapped-ion cell. Peak pressure during the trapping event is typically 5×10^{-6} torr, and analyzer base pressure is restored in 20–30 s. Amplification of the 0–10-V trap driver in the Odyssey cell controller allows potentials up to 30 V to be used for accumulation of higher energy ions.

Ion radial excitation is typically accomplished with a broadband frequency sweep, and the resulting transients are digitized at up to 2M data points per spectrum. This large memory capacity allows 6-s acquisitions at a bandwidth of 150 kHz, corresponding to a lower mass limit of m/z 600. Standard heterodyne techniques [34] were used to acquire for longer periods for ultrahigh-resolution measurements.

All compounds were obtained from Sigma Chemical Co. (St. Louis, MO) and used without further purification. Equine cytochrome *c* (12.3 kDa) was used for all ion injection studies unless otherwise noted.

Ion Injection

The ion generation and injection process results in some residual axial ion kinetic energy on arrival at the cell. It is important that this energy be known and minimized to design effective trapping techniques. Retarding potential studies of an injected ion beam comprising the full charge-state envelope of cytochrome *c* ions (+16 to +7) with a 20-V offset on the first quadrupole lens indicate that the ion energy distribution is approximately Gaussian, with a maximum at approximately 15 eV per charge and a full width at half maximum of approximately 12 eV per charge. Similarly, the average energy per charge is always somewhat less than the quadrupole potential offset at both higher and lower voltages, consistent with collisional retardation in this approximately 10^{-4}-torr region. This relatively wide apparent kinetic energy per unit charge distribution, as determined by a retarding potential study, may be attributed to a variety of effects. For example, if all of the ions from the +16 to +7 charge-state envelope of cytochrome *c* are accelerated to the same velocity of 1000 m/s in the supersonic expansion of the ESI source, then the retarding potential profile would extend from 4 to 9 V, even though all of the ions have the same kinetic energy. This is a simple consequence of the fact that the retarding force experienced by the ions is proportional to the charge on the ion. Convoluting the energy distribution that results from electrostatic acceleration in a high-pressure region with the wide distribution of ion charge states and the distribution of velocities gained in the supersonic expansion yields a wide apparent distribution of ion energies. Additional contributions to the distribution are encountered on injecting ions with a distribution of radial energies acquired in the quadrupole lenses, through the strong magnetic field gradient of the superconducting magnet (the well-known magnetic mirror effect). Because the width of the kinetic energy per unit charge distribution can have an important effect on overall trapping efficiency (see Ion Trapping), there is a continuing effort to find a combination of source and injection parameters that will minimize this distribution. To facilitate trapping for a given distribution width, it is similarly important to minimize the energy per charge corresponding to the distribution maximum, a parameter principally controlled in this instrument by the offset potential on the first quadrupole. A higher offset potential on this element yields more efficient ion injection; however, in practice an offset of 10–20 V results in the best compromise between high-efficiency injection and low residual ion energy.

Ion Trapping

Two approaches are common for collecting externally generated ions in the cell—gated and accumulated trapping [37]. Gated trapping involves lowering the applied potential at either end of the cell to allow ions into the cell and then raising the potential to retain the ions. This technique requires that the ion energy be lower than the available trapping potentials and is

most effective for pulsed-ion production. For our continuous-ionization instrument, accumulated trapping, such as used by Laude and co-workers [37, 38], has been much more effective. Static trapping potentials are maintained while injecting ions with kinetic energy sufficient to penetrate the trapping field; deceleration in the cell traps the ions between the static potentials. The most likely deceleration mechanism is collision with neutral gas molecules, which has proved effective in higher pressure external source instruments [38]. In fact, at pressures lower than approximately 10^{-8} torr, accumulation is essentially undetectable. Determination of total accumulated ion abundance as a function of static analyzer pressure (from leak-valve introduction of nitrogen) indicates that accumulation increases dramatically with pressure up to 10^{-6} torr. Beyond this range, collisional scattering, space-charge effects, and other losses apparently offset improved trapping. Such effects can be minimized by providing high pressures only during the ion injection event. Thus, pulsed-gas introduction during ion injection proved to be a convenient way to increase the trapping efficiency; peak pulse pressures of approximately 10^{-5} torr with injection times of less than 1 s require approximately 20 s to restore the base pressure required for high-performance excitation and detection of the acquired ions. Although sufficient ion populations are easily acquired with this technique, overall trapping efficiency is quite low. Using a statistical method to estimate the number of ions in the cell [39], a typical trapping efficiency of only 0.1% is calculated based on the measured cell current and ion injection period.

Consistent with the results of Hofstadler and Laude [38], the effect of trapping potential on total ions accumulated generally mimics the kinetic energy profile of the injected ion population. Because the ions are required to traverse the 10-cm distance between the injection quadrupole and cell during the high-pressure injection event, some ion deceleration occurs prior to arrival at the cell, and thus the optimum trapping potential may be as much as a few volts lower (depending on the pressure used for trapping) than would be indicated by the energy distribution measured at low pressure. Although relatively high trapping potentials are required for optimum accumulation, most of the ion kinetic energy was damped sufficiently within 1 s for the ions to be retained with much lower trapping potentials (typically ≤ 1 V). Thus, following ion injection, the potential is stepped down to this range to minimize trapping potential-induced frequency shifts and to promote optimum ion detection. Experiments with ramped-down rather than stepped changes provided no improvement in subsequent detection, and thus the simpler stepped change is used in this work.

As was observed with Laude and co-workers' [38, 40] internal electrospray instrument, the efficiency of acquisition with this instrument also varies with charge state as well as with trapping potential. The total ion kinetic energy is the sum of a component from the supersonic expansion in the source, in which each ion is accelerated to the same velocity and energy-dependent on mass and collision cross section but independent of charge, and an electrostatic component from acceleration between lens elements of different potential to add a constant energy per unit charge. Thus, the total energy per unit charge varies, and the extent of this determines the variation in optimum trapping potential per number of charges. For example, a more highly charged ion will require a lower trapping potential than a less charged ion of the same kinetic energy because the force experienced by an ion in a given electric field is proportional to the charge on the ion. These effects have recently been explored in some detail, and the mass-to-charge discrimination that results from such effects has been demonstrated to provide a method for selective mass and charge-state acquisition of electrosprayed ions [40]. Such capability appears to be a general feature of the ESI/FT/MS experiment, independent of the manner in which ions are introduced to the cell.

The extent of initial ion deceleration during the trapping process may be probed by varying the potential difference between the rear and front trap plates (Figure 2). Ions with sufficient energy to penetrate the first trap must lose enough kinetic energy during their passage through the cell to be retained by the rear trap

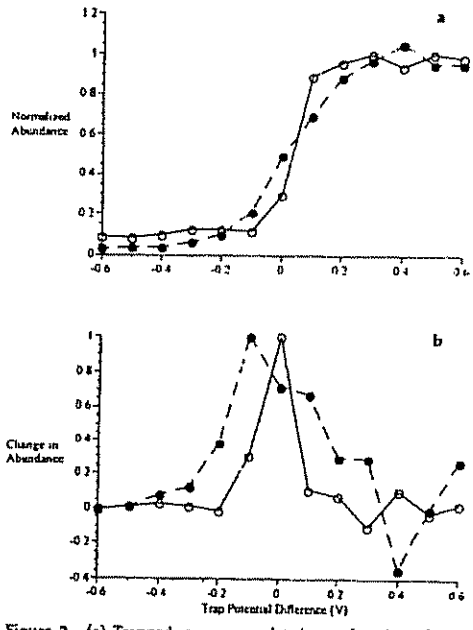

Figure 2. (a) Trapped ions accumulated as a function of trap plate potential difference, static cell pressure. (○) 3×10^{-7} torr, (●) 6×10^{-7} torr. (b) Differential of trap plate potential difference profile shown in a

TA 118

T005886

potential. The steeper curve at the lower pressure in Figure 2a is consistent with less (and a narrower range of) ion energy lost during the initial cell traversal, as expected. This is shown more clearly in differential form in Figure 2b, minimizing the width of the final axial kinetic energy distribution of the acquired ions has been found to promote high-resolution measurements. However, even at the higher pressure, it is apparent that the accumulated trapping technique retains a relatively narrow "slice" (< 0.5 eV per charge) of the injected kinetic energy per unit charge distribution. It is for this reason that it is desirable to minimize the width of that distribution and thus maximize the population density within the acquired energy interval.

High Resolution

It is well known [31–33] that the higher field magnet and lower system pressure from the larger capacity pumping system should improve performance; however, factors that affect transient lifetimes and field homogeneities are also important. The support structure for the original trapped-ion cell exhibited an unusually large magnetic susceptibility, so this was replaced with a laboratory-built copper open cell [36]. The open geometry is inherently more compatible with external ion injection, as well as providing lower electric field inhomogeneities. It was also found that cell and cell lead vibrations, as well as low-frequency noise in the detection circuitry, resulted in reduced ion storage time and shorter transients; such excitation of low-frequency (trapping and magnetron) modes could promote ion cloud expansion and ion loss. Finally, low trap potentials ($\leq$ 1 V), ion cooling delays (usually 120 s), and small ion populations were found to improve transient lifetimes significantly. Space-charge effects imposed by the density of the ion population are perhaps the most significant factor and require a careful compromise between the objectives of high signal-to-noise ratio and high resolution to achieve spectra (Figures 3 and 4) of 8.6–29-kDa proteins of 2–0.5 $\times$ 10^6 resolving power.

Figures 3 and 4 show three examples of high-resolution spectra acquired with the new instrument. Figure 3a is a high-resolution spectrum of bovine ubiquitin (8565 Da), with a resolving power of 2 $\times$ 10^6. This spectrum was collected with a 0.5-s ion beam injection period (250 fmol injected), with 13 and 14 V on the front and rear trap plates, respectively, during the beam event. The trap potentials were then decreased to 1 V, and the ions were cooled for 120 s. Excitation was then performed using a chirp from 50 to 150 kHz at a sweep rate of 100 Hz/μs; 2M data points were then collected in heterodyne mode at a bandwidth of 35 kHz, corresponding to m/z 770–1075. (Although the signal acquisition period was 30 s, the transient lifetime in this example was only approximately 20 s, and thus resolution is not data-point limited.) The

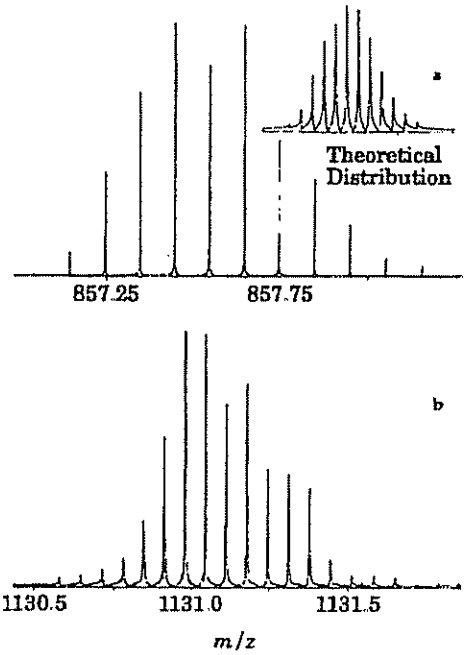

Figure 3. Single-scan partial mass spectrum of (a) ubiquitin (8565 Da), resolving power 2 $\times$ 10^6, and (b) apomyoglobin (16,952 Da), resolving power 9 $\times$ 10^5.

central peak in the isotopic cluster appears smaller than the adjacent peaks because the two highest points on the peak are at the same abundance and by chance symmetrically disposed about the peak maximum, making the peak appear flat-topped. Zero filling the data before processing would improve the appearance of the isotopic profile, but this is not possible on the

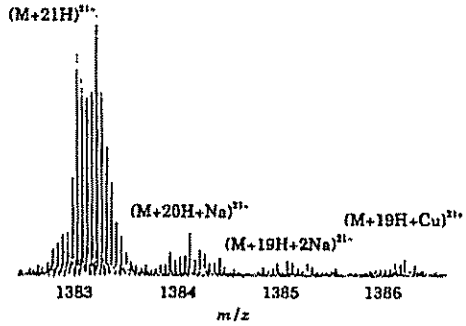

Figure 4. Single-scan partial mass spectrum of carbonic anhydrase (29,025 Da), resolving power 5 $\times$ 10^5.

current data system for a 2M point spectra owing to memory limitations.

Figure 3b is a comparable spectrum of horse skeletal muscle apomyoglobin (16,952 Da) recorded at 9×10^5 resolving power. The conditions were the same as in Figure 3a, except that a 1-s beam was used (0.5 pmol), with a 75-Hz/μs sweep rate and a bandwidth of 79 kHz, covering the range m/z 750–2000. The irregular shape of the isotopic envelope is attributed to small population ion statistics. With at most a few thousand ions contributing to the entire isotopic profile, there will be significant random fluctuations from the theoretical abundances.

Figure 4 is a spectrum of bovine carbonic anhydrase II (29,025 Da) recorded at a resolving power of 5×10^5. Experimental conditions were the same as in Figure 3, except that a 2-s beam was used (1 pmol), and only 1M data points were collected, thus making the resolving power data-point limited. With this signal-to-noise level, both sodium and copper adducts are visible in the spectrum. These adduct assignments are confirmed by accurate mass measurements and by doping the samples with the corresponding acetate salt, which increases the abundance of the corresponding adduct peaks. The copper ions result from the reaction of acidic sample solutions with exposed brass in the nickel-plated brass fittings of the sample syringe [20].

The effect of static system pressure (nitrogen) on resolution was determined for spectra of cytochrome *c*. Isotopic resolution is lost at 6×10^{-3} torr, although with D_2O, a lower mass gaseous neutral, isotopic resolution can still be obtained at 10^{-7} torr (Figure 5) [24].

Theory predicts that resolving power should decrease with increasing mass-to-charge ratio, even for ions of the same mass value, when not under pressure-limited conditions. Figure 6 shows the resolving power measured for cytochrome *c* versus mass-to-charge (closed circles), whereas the line represents the predicted reciprocal relationship. This gratifying agreement is in contrast to recent higher pressure measurements of Hofstadler and Laude [38] in which the isotope peaks were not resolved, so that observed peak widths are dominated by the width of isotope distribution profiles. In fact, only under high-pressure (10^{-6}-torr range) conditions is the resolving power observed to increase rather than decrease with increasing mass-to-charge for ions of the same mass. This increase is linear with mass-to-charge, consistent with resolution decreased by collisional damping, with the collision rate determined by ion velocity, which decreases linearly with increasing mass-to-charge.

It is important to note that although long transient lifetimes are a prerequisite for obtaining high resolution, such lifetimes alone are not a sufficient condition. If during the evolution of the transient the ions experience a variation in the magnetic field or nonquadrupolar variation in the electric field, there will be a corresponding shift in the effective cyclotron frequency during the transient. Such a continuous frequency shift

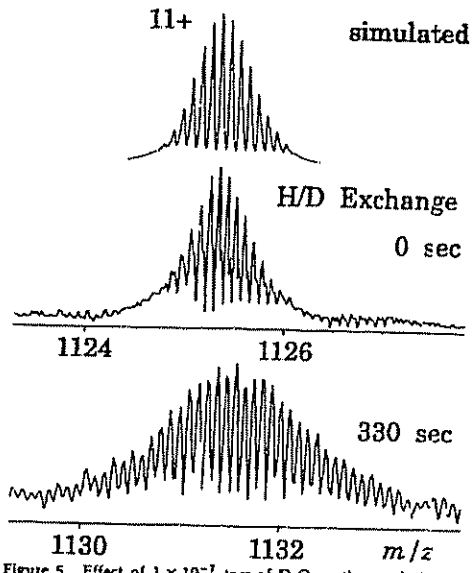

Figure 5. Effect of 1×10^{-7} torr of D_2O on the resolution of cytochrome *c* with H/D exchange

will cause a corresponding broadening of peaks. To the extent that the transient decay of such large ions represents a corresponding decay in the radial amplitude of ion motion [25] rather than a dephasing of coherent ion motion, radial field inhomogeneities should be the primary cause of frequency shifts during the transient. Radial magnetic field inhomogeneities may exist owing to intrinsic problems with the magnet, nonoptimum positioning of the cell, or the use of high-susceptibility materials for cell or cell support construction. Nonquadrupolar electric fields are likely to be experienced whenever the radial amplitude of ion motion exceeds about one half of the cell radius or

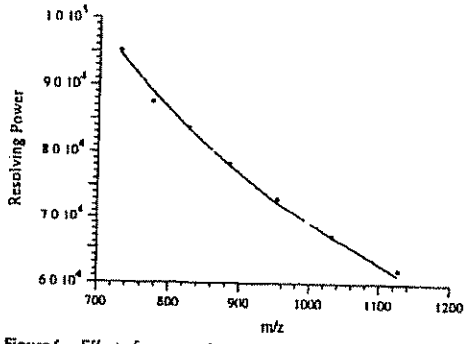

Figure 6. Effect of mass-to-charge ratio value on resolving power for cytochrome *c* (12,361 Da) isotopic peaks: (●) measured values; (—) theoretically predicted function. The letters indicate the amino acid composition of fragments.

when ion population densities are large enough to cause significant Coulombic interaction between ions. Regardless of the cause, such frequency shifts will be evidenced by a frequency resolution that does not correspond to the inverse of transient lifetime; the highest resolution may then be obtained for observation times significantly shorter than the transient decay time. This effect may be used as a simple diagnostic tool for probing field inhomogeneities in the trapped-ion cell.

Although these advances in high resolution allow mass determinations with errors of less than 0.1 Da, there is still the potential to make an error of ±1 Da from an incorrect assignment for the number of heavy isotopes present in a specific peak. This is not a problem for smaller ions because the peak of lowest mass must be monoisotopic; however, its intensity decreases as mass increases because of the increased probability for multiple heavy isotopes. For ubiquitin, the monoisotopic peak abundance is less than 4% of that of the most abundant peak (Figure 3a). The monoisotopic mass of a molecule can be estimated using the average molecular weight from the unresolved isotopic cluster [41].

For resolved isotopic peaks, their measured intensity profile can be compared with a model theoretical profile to assist in the assignment for the monoisotopic mass. The profile expected as a function of protein molecular weight was derived from the statistical occurrence of elemental composition of the amino acids from the Protein Identification Resource (National Biomedical Research Foundation, Washington, DC) protein data base. Using the measured average molecular weight of a compound, the theoretical isotopic profile is calculated [42]. To improve the precision of abundance values, isotopic profiles from multiple charge states are convoluted [43]. Details of the method and its successful routine application are reported elsewhere [39].

This instrument configuration with its unusual capabilities for high-resolution measurements of large ions has several potential advantages. These include determination of the charge state of unknown ions based on ^{13}C isotopic spacing [21–23], observation of low-mass adducts on large molecules (Figure 4), improved tracking of isotope-exchange reactions [24], improved mass accuracy (< 1 ppm) for isotopically resolved peaks [20], and distinguishing isobaric elemental composition assignments (glutamine and lysine contribute 128.058 and 128.095 Da, respectively, to the protein mass, so that 1-ppm mass accuracy will distinguish these at 20 kDa).

Ion Dissociation

Further characterization of MS-I-analyzed ions from ESI requires an effective ability for their dissociation and/or reaction. Of our initial dissociation studies, collisionally activated dissociation (CAD) of the radially excited ions was not found to be effective for peptides larger than gramicidin S (1.2 kDa) despite success in triple quadrupole CAD experiments with 66-kDa albumin ions [19]. Photodissociation using a 193-nm laser (Figure 1) is more effective for gramicidin S (Figure 7) and 8.6-kDa ubiquitin (Figure 8) but produces predominantly small, less informative fragments that are difficult to assign because of apparent internal fragmentations. Photodissociation of larger ions did not yield observable products, even though the parent ion abundance decreased with increasing irradiance. Attempts to trap the presumably high kinetic energy fragments using higher trap potentials and/or pulsed-gas collisional cooling were unsuccessful. By far the best dissociation results were obtained with nozzle/skimmer dissociation in the external ion source [18–20], as demonstrated (Table 1) for ubiquitin (Figure 9) and carbonic anhydrase (Figure 10). Here some of the lower abundance fragments of ubiquitin exhibit peak splitting that resembles an overlapping isotope distribution. This splitting is eliminated when smaller ion populations are used (for example, by ejecting higher abundance ions) and thus is apparently caused by space-charge effects. For carbonic anhydrase, the masses of 38 fragment ions could be assigned directly from their isotopic spacing, with 15 of these corresponding to terminal fragments of the known sequence. Nozzle/skimmer dissociation thus appears to be quite effective in dissociating larger ions and further provides abundant large-fragment ions (5–10 kDa) that may prove to be amenable to further dissociation in the trapped-ion cell by conventional CAD or photodissociation techniques. A disadvantage of the nozzle/skimmer technique is that it indiscriminately dissociates all electrosprayed ions, forfeiting the significant MS/MS advantage of selectivity.

The trapped-ion capabilities of FTMS also allow characterization of the mass-analyzed primary ions by ion–molecule reactions. For example, H/D exchange

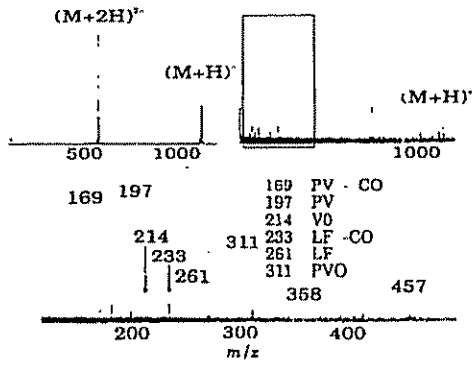

Figure 7. Photodissociation (193 nm) of gramicidin S ions before and after 25 laser shots. The letters indicate the amino acid composition of fragments.

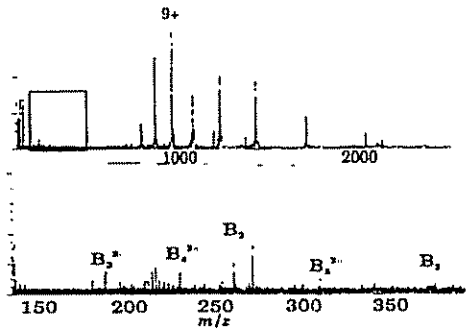

Figure 8. Photodissociation (193 nm) of ubiquitin ions (8565 Da), 10 scans.

Table 1. Assigned dissociation fragments for ubiquitin and carbonic anhydrase

Fragment	Charge	m/z
Ubiquitin		
y_{24}	4, 3	683, 910
y_{18}	3, 2	700, 1050
y_{38}	9, 8, 7	727, 818, 935
b_{16}	2	904
b_{18}	2	1018
Carbonic anhydrase		
y_{24}	4	741
b_{31}	4	912
b_{40}	5	924
y_{67}	8, 7, 6	951, 1087, 1268
y_{25}	3	987
y_{61}	7, 6, 5	1007, 1175, 1410
b_{135}	15	1022
y_{76}	8, 7	1095, 1251
y_{63}	6	1208
y_{68}	6	1295

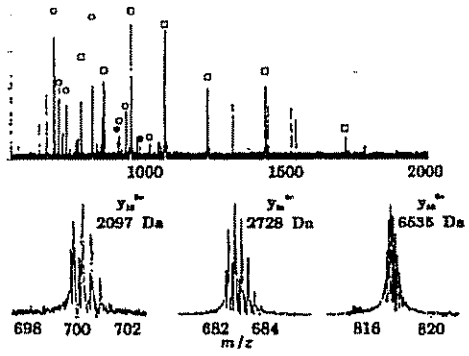

Figure 9. Nozzle/skimmer (150 V) dissociation of ubiquitin ions: (○) y-type ions; (●) b-type ions; (□) molecular ions.

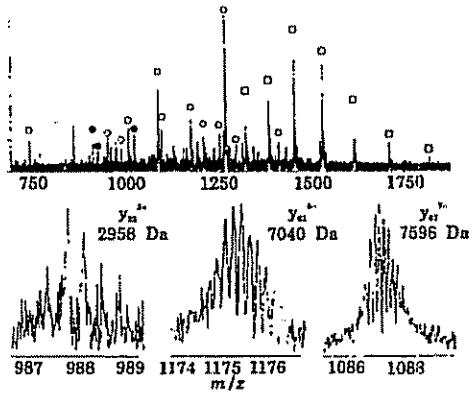

Figure 10. Nozzle/skimmer dissociation of carbonic anhydrase ions (29.0 kDa); symbols as in Figure 9.

with multiply charged protein ions by D_2O, CH_3OD, CH_3COOD, and ND_3 have demonstrated the stability of multiple three-dimensional conformers [24].

Conclusions

The triple quadrupole [6, 44] and the tandem double-focusing magnetic sector instruments [4, 5, 45] are now recognized as unique tools for providing definitive molecular weight and sequence information on oligopeptides (< 3 kDa), even in subpicomole amounts and as components of mixtures. The FTMS instrument described here could be the forerunner of a new generation of mass spectrometers, providing such information on biomolecules larger by one or even two orders of magnitude and using samples smaller by ever three orders of magnitude.

Acknowledgments

We are grateful to J. E. Campana, J. B. Fenn, M. L. Gross, D. F. Hunt, J. A. Loo, J. Shabanowitz, A. Siapikas, B. H. Wang, C. M. Whitehouse, C. L. Wilkins, E. R. Williams, and M.-Y. Zhang for valuable help.

We thank the National Institutes of Health (Grant GM16609) and the Gavlin Foundation for generous financial support.

References

1. Biemann, K. *Mass Spectrometry: Organic Chemical Applications*; McGraw-Hill: New York, 1962; pp 283–296.
2. Senn, M.; Venkataraghavan, R.; McLafferty, F. W. *J. Am. Chem. Soc.* 1966, *88*, 5593.
3. Biemann, K.; Cone, C.; Webster, B.; Arsenault, G. P. *J. Am. Chem. Soc.* 1966, *88*, 5598.
4. Biemann, K. *Biomed. Environ. Mass Spectrom.* 1988, *16*, 99–111.
5. Carr, S. A.; Hemling, M. E.; Bean, M. F.; Roberts, G. D. *Anal. Chem.* 1991, *63*, 2802–2824.

6. Hunt, D. F.; Michel, H.; Dickenson, T. A.; Shabanowitz, J.; Cox, A. L.; Sakaguchi, K.; Appella, E.; Gray, H. M.; Sette, A. *Science* 1992, *256*, 1817–1820.
7. McLafferty, F. W.; Venkataraghavan, R.; Irving, P. *Biochem Biophys. Res Commun.* 1970, *39*, 274.
8. Wipf, H.-K.; Irving, P.; McCamish, M.; Venkataraghavan, R.; McLafferty, F. W. *J. Am. Chem. Soc.* 1973, *95*, 3369.
9. Cody, R. B. Jr.; Amster, I. J.; McLafferty, F. W. *Proc. Natl Acad. Sci. USA* 1985, *82*, 6367–6370.
10. Levsen, K.; Wipf, H.-K.; McLafferty, F. W. *Org. Mass Spectrom.* 1974, *8*, 117.
11. Macfarlane, R. D.; Hill, J. C.; Jacobs, D. L.; Phelps, R. G. In *Mass Spectrometry in the Analysis of Large Molecules*, McNeal, Ed.; John Wiley: New York, 1986; pp 1–12.
12. Barber, M.; Bordoli, R. S.; Sedgwick, R. D.; Tyler, A. N. *J. Chem. Soc., Chem. Commun.* 1981, *3*, 25.
13. Hillenkamp, F.; Karas, M.; Beavis, R. C.; Chait, B. T. *Anal. Chem.* 1991, *63*, 1193A–1202A.
14. Clegg, G. A.; Dole, M. *Biopolymers* 1971, *10*, 821–826.
15. Fenn, J. B.; Mann, M.; Meng, C. K.; Wong, S. F.; Whitehouse, C. M. *Science* 1989, *246*, 64–71.
16. (a) Smith, R. D.; Loo, J. A.; Ogorzalek Loo, R. R.; Busman, M.; Udseth, H. R. *Mass Spectrom. Rev.* 1991, *10*, 359–451; (b) Smith, R. D.; Loo, J. A.; Ogorzalek Loo, R. R.; Busman, M.; Udseth, H. R. *Mass Spectrom. Rev.* 1992, *11*, 434–443.
17. Griffin, L. L.; McAdoo, D. J. *J. Am. Soc. Mass Spectrom.* 1993, *4*, 11–15.
18. Loo, J. A.; Udseth, H. R.; Smith, R. D. *Rapid Commun. Mass Spectrom.* 1988, *2*, 207–210.
19. Loo, J. A.; Edmonds, C. G.; Smith, R. D. *Anal. Chem.* 1991, *63*, 2488–2499.
20. Beu, S. C.; Senko, M. W.; Quinn, J. P.; McLafferty, F. W. *J. Am. Soc. Mass Spectrom.* 1993, *4*, 190–192.
21. Henry, K. D.; McLafferty, F. W. *Org. Mass Spectrom.* 1990, *25*, 490–492.
22. Henry, K. D.; Quinn, J. P.; McLafferty, F. W. *J. Am. Chem. Soc.* 1991, *113*, 5447–5449.
23. Loo, J. A.; Quinn, J. P.; Ryu, S. I.; Henry, K. D.; Senko, M. W.; McLafferty, F. W. *Proc. Natl Acad. Sci. USA* 1992, *89*, 286–289.
24. Suckau, D.; Shi, Y.; Beu, S. C.; Senko, M. W.; Quinn, J. P.; Wampler, F. M. III; McLafferty, F. W. *Proc. Natl. Acad. Sci. USA* 1993, *90*, 790–793.
25. Williams, E. R.; Henry, K. D.; McLafferty, F. W. *J. Am. Chem. Soc.* 1990, *112*, 6157–6162.
26. Freiser, B. S.; Jacobson, D. B. *Science* 1984, *112* (cover page).
27. Comisarow, M. B.; Marshall, A. G. *Chem. Phys. Lett.* 1974, *25*, 282–283.
28. White, R. L.; Ledford, E. B.; Ghaderi, S.; Wilkins, C. L.; Gross, M. L. *Anal. Chem.* 1980, *52*, 252.
29. Castro, M. E.; Russell, D. H. *Anal. Chem.* 1984, *56*, 578.
30. Cody, R. B. Jr.; Kinsinger, J. A.; Ghaderi, S.; Amster, I. J.; McLafferty, F. W.; Brown, C. E. *Anal. Chim. Acta* 1985, *178*, 43–66.
31. Buchanan, M. V., Ed. *Fourier Transform Mass Spectrometry*, American Chemical Society: Washington, D.C., 1987.
32. Wilkins, C. L.; Chowdhury, A. K.; Neuwaysir, L. M.; Coates, M. L. *Mass Spectrom. Rev.* 1989, *8*, 67–92.
33. Marshall, A. G.; Grosshans, T. B. *Anal. Chem.* 1992, *63*, 215A–229A.
34. Marshall, A. G.; Schweikard, L. *Int. J. Mass Spectrom. Ion Processes* 1992, *118/119*, 37–70.
35. Chowdury, S. K.; Katta, V.; Chait, B. T. *Rapid Commun. Mass Spectrom.* 1990, *4*, 81–87.
36. Beu, S. C.; Laude, D. A. Jr. *Int. J. Mass Spectrom. Ion Processes* 1992, *112*, 215–230.
37. Beu, S. C.; Laude, D. A. Jr. *Int. J. Mass Spectrom. Ion Processes* 1992, *104*, 109–127.
38. Hofstadler, S. A.; Laude, D. A. Jr. *J. Am. Soc. Mass Spectrom.* 1992, *3*, 615–623.
39. Senko, M. W.; Beu, S. C.; McLafferty, F. W., to be submitted.
40. Hofstadler, S. A.; Beu, S. C.; Laude, D. A. Jr. *Anal. Chem.* 1993, *65*, 312–316.
41. Zubarev, R.; Bonarenko, P. *Rapid Commun. Mass Spectrom.* 1991, *5*, 276–277.
42. Yergey, J. *Int. J. Mass Spectrom. Ion Phys.* 1983, *52*, 337–349.
43. Labowsky, M.; Whitehouse, C.; Fenn, J. B. *Rapid Commun. Mass Spectrom.* 1993, *7*, 71–84.
44. Yost, R. A.; Enke, C. G. In *Tandem Mass Spectrometry*, McLafferty, F. W., Ed., John Wiley: New York, 1983; pp 175–195.
45. McLafferty, F. W.; Todd, P. J.; McGilvery, D. C.; Baldwin, M. A. *J. Am. Chem. Soc.* 1980, *102*, 3360–3363.